ACS MATERIALS LETTERS

www.acsmaterialsletters.org

Vertically Aligned Nanoplates of Atomically Precise Co_6S_8 Cluster for Practical Arsenic Sensing

Anagha Jose, Arijit Jana, Tanvi Gupte, Akhil S. Nair, Keerthana Unni, Ankit Nagar, Amoghavarsha R. Kini, B. K. Spoorthi, Sourav Kanti Jana, Biswarup Pathak,* and Thalappil Pradeep*

Cite This: *ACS Materials Lett.* 2023, 5, 893–899

Read Online

ACCESS | Metrics & More | Article Recommendations | Supporting Information

ABSTRACT: **Two-dimensional nanostructures with atomically precise building blocks have potential applications in catalysis and sensing. However, structural instability and surface reactivity limit their practical use. In this work, we demonstrate the formation of vertically aligned nanoplates of the $[Co_6S_8DPPE_6Cl_6]$ cluster (Co_6 in short), protected by 1,2-bis(diphenylphosphino)ethane, using ambient electrospray deposition (ESD). Charged microdroplets of Co_6 formed by ESD on a water surface created such nanostructures. Preferential arrangement of clusters in the nanoplates with enhanced surface area results in sensitive and selective electrochemical response toward arsenite down to 5 parts per billion, in tap water. Density functional theory calculations reveal the preferential binding of arsenite with Co_6. Our work points to a practical application of atomically precise clusters of large societal relevance.**

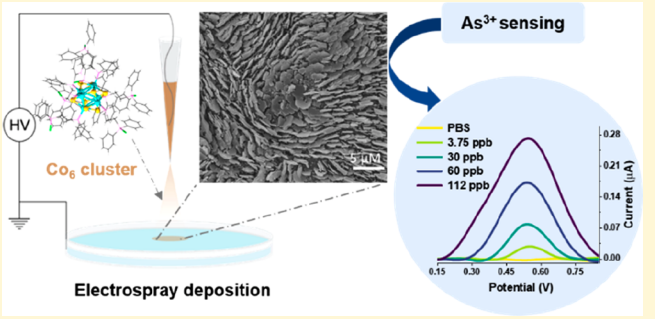

INTRODUCTION

Atomically precise clusters of noble metals, metal oxides, and chalcogenides are expanding the boundaries of materials chemistry.[1−8] Quantized electronic structures due to atomic confinement leading to new photophysical, chemical, catalytic, and magnetic properties of these materials have resulted in several advancements.[9−16] One of the obvious areas of their impact is in sensors due to the possibility of a large number of accessible surface sites and the ability to tune the sensitivity of analytes to their varying electronic structure.[17] As a result, optical and fluorescence sensors to detect chemical, biochemical, and elemental species have been reported.[18−22] However, the use of such sensors in practical applications has been lacking either due to the reduced stability of such systems, selectivity toward analytes, limits of analysis, or cost.[23] Therefore, atomically precise clusters, synthesized from inexpensive precursors and with superior stability, are essential for expanding the utility of these materials.

Arsenic in drinking water affects over 120 million people worldwide, and its grip is expanding continuously due to the excessive use of groundwater, fertilizers, and agrochemicals.[24,25] A practical arsenic sensor in water without the need for preconcentration and sophisticated instrumentation is very much in need. Key to developing such practical electrochemical devices for arsenic is the development of stable, selective, sensitive, and affordable electrodes.[26,27] Increased sensitivity requires the electrode to be composed of specific chemical species with morphologies or superstructural microcrystalline assemblies, enhancing the specific surface areas.[28−30] In view of the sensitivity of cobalt-based systems for arsenic sensing,[31] we decided to explore the atomically precise Co_6 cluster system to develop a practical sensor. We have developed a method of ambient electrospray deposition (ESD) of the Co_6 cluster system leading to their 2D nanostructures with unique morphologies.[32−34] In this work, we present a practical electrochemical arsenic sensor based on the resulting structures for arsenite detection down to 5 parts per billion (ppb) in tap water implementable in field applications. As the safe limit of arsenic in drinking water is 10 ppb, and the detection is demonstrated in tap water, practical application of such materials is possible. Cost per analysis is estimated to be less than $1 per measurement.

Received: January 27, 2023
Accepted: February 17, 2023
Published: February 22, 2023

https://doi.org/10.1021/acsmaterialslett.3c00085
ACS Materials Lett. 2023, 5, 893–899

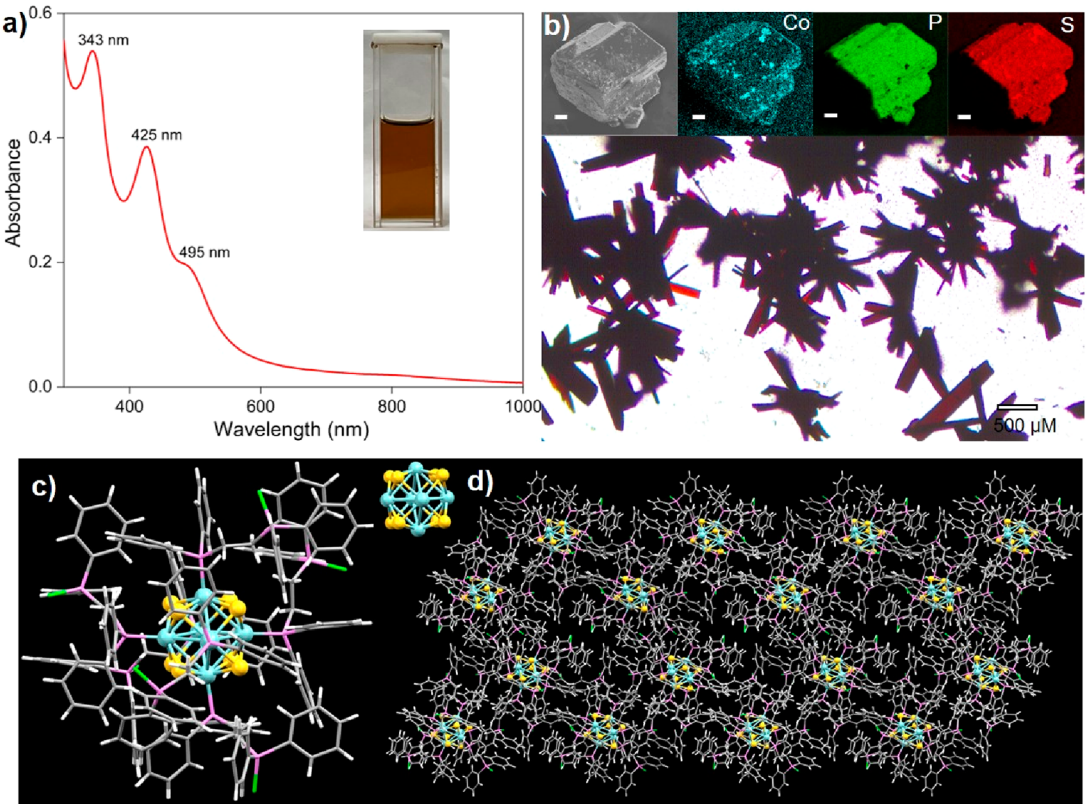

Figure 1. (a) UV−vis absorption spectrum of Co_6 in DCM (inset shows the photograph of the respective solution). (b) Optical microscopic image of the crystals (inset shows the FESEM micrograph of a crystal and the respective elemental mapping; scale bar corresponds to 500 nm). (c) Molecular structure of the cluster including ligands (inset shows the Co_6S_8 core, with an octacapped octahedron geometry). (d) Large area supramolecular packing of $[Co_6S_8DPPE_6Cl_6]$ in the *b* plane. Atomic color codes for c and d: cyan = cobalt, yellow = sulfur, pink = phosphorus, green = chlorine, gray = carbon, and white = hydrogen.

RESULTS AND DISCUSSION

The Co_6 cluster was synthesized using a reported protocol[35] with a different ligand, namely, 1,2-bis(diphenylphosphino)-ethane (DPPE; detailed synthetic procedure is given in the SI). The as-synthesized cluster in dichloromethane (DCM) was brownish in color and exhibited well-defined optical absorption peaks in a characteristic pattern emphasizing its molecular nature (Figure 1a). The stability of the cluster was monitored using time-dependent UV−vis in solution, and no change was seen up to 60 days under ambient conditions (Figure S1). We have observed almost identical absorption features in multiple solvents (Figure S2). Cuboidal single crystals of the cluster were grown in 7 days from a saturated DCM solution upon layering with hexane at 4 °C (Figure 1b). Field emission scanning electron microscopic (FESEM) images of the crystal (shown in the inset of Figure 1b) correlate with the optical micrograph. Energy-dispersive spectroscopy (EDS; Figure S3) and elemental mapping of the crystals (shown in the inset of Figure 1b) confirm the presence of Co, S, P, and Cl in them. Single crystal X-ray diffraction (SCXRD) measurements gave the structural framework of the cluster shown in Figure 1c. It exhibited a monoclinic unit cell with the space group of P21/c (detailed crystallographic information is given in Table S1 and S2). The core of the cluster is arranged in an octahedral fashion with six Co atoms, having an average Co−Co bond length of ∼2.8 Å. Each triangular face of the Co_6 octahedron is further protected by eight isolated S atoms, resulting in an octacapped octahedral geometry (shown in the inset of Figure 1c). The average Co−S bond length is ∼2.2 Å and each S sits ∼1.5 Å away from the centroid of the respective Co_3 faces (shown in Figure S4). A bond length analysis shows strong metal−metal and metal−sulfide interactions, which provide rigidity to the kernel of the cluster.

Six bidentate DPPE ligands protect the cluster; one phosphine end of DPPE is directly bonded to the cobalt, and the other end binds with the chlorine resulting in average Co−P and P−Cl bond lengths of 2.12 and 2.48 Å, respectively. Supramolecular packing of the cluster reveals that four clusters are packed inside the unit cell (Figure S5). Large area packing shows the AB···AB kind of packing of the clusters (Figure 1d) through CH-π, CH-Cl, CH-P, and Cl-π interactions (Figure S6). High resolution electrospray ionization mass spectrometry (HRESI-MS) of the cluster showed a peak at m/z 3213.96 in the positive ion mode, in the singly charged state, which corresponds to the composition of the cluster $[Co_6S_8(DPPE)_6Cl_6]$ as revealed by SCXRD (Figure S7). The presence of these elements has been further verified using X-ray photoelectron spectroscopy (XPS; Figure S8). Experimental X-ray diffraction patterns obtained from the crystalline samples of Co_6 cluster were in good agreement with the simulated data (shown in Figure S9). The strong appearance of 6.21, 6.42, 6.6, 7.19, 8.15, 11.6, and 14.83 diffraction peaks in the 5−15° 2θ range correspond to (012), (110), (102), (11−2), (004), (122) and (116) lattice planes, respectively. However, several features were not clearly visible due to their poor intensities. Some intensity variations were also seen. Thermogravimetric (TG) and differential thermogravimetric (DTG) analysis of microcrystalline Co_6 was carried out for the

https://doi.org/10.1021/acsmaterialslett.3c00085
ACS Materials Lett. 2023, 5, 893−899

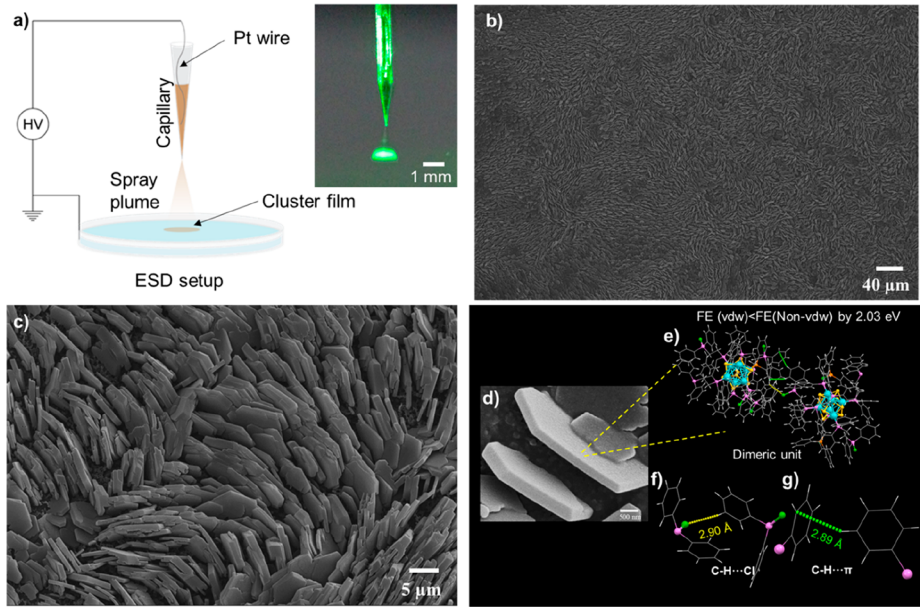

Figure 2. (a) Schematic representation of our home-built electrospray setup. Inset shows a photographic image of the nanospray plume generated from the tip of the capillary. The plume is visualized using a green laser, which scatters from it. (b) Large area and (c) magnified FESEM micrographs of the vertically aligned nanoplates. (d) An expanded image of microcrystalline hexagonal nanoplates. (e) Intercluster interaction leading to such a superstructure. (f, g) Ligand-centered short contact interactions between two clusters.

heating range from 25 to 700 °C. No mass loss was observed up to 400 °C, suggesting superior thermal stability in the solid state (Figure S10).

Time-dependent density functional theory (TD-DFT) calculations (see details in SI) were carried out to obtain an atomistic understanding of the optical properties of $[Co_6S_8(DPPE)_6Cl_6]$.[36] The obtained theoretical absorption spectrum is in agreement with the experimental spectrum (Figure S11a). The frontier molecular orbital (FMO) analysis revealed the contribution of the molecular orbitals corresponding to 321, 427, and 498 nm (Figure S11b). Projected density of states (PDOS) analysis indicates that the occupied states have major contributions from Co(d) states and P(sp) states, whereas the unoccupied states are mainly occupied by S(sp) and Cl(sp) states centered at the ligands encapsulating the Co_6 kernel (Figure S11c). This is further supported by the Kohn–Sham orbital analysis (Figure S11d). However, we note that the HOMO and LUMO states have a higher contribution from the ligands than the Co_6 kernel indicating the significant role of ligands in governing the electronic properties of the cluster (Figure S12).

We created self-assembled superstructures of the cluster using the ESD technique. A schematic of our home-built ESD setup is shown in Figure 2a. The cluster solution in DCM was sprayed as solvated microdroplets through a glass capillary tip (diameter 30–35 μm) by applying a positive potential of 2.75–3 kV (photograph of spray plume is shown in the inset of Figure 2a) at a flow rate of 30 μL h^{-1}. After 30 min of continuous deposition of such charged microdroplets onto an ultrapure water substrate, a brownish thin film resulted, floating on it. From our previous report, the spray current measured between the tip and the substrate was 40 nA.[32] The obtained film was carefully transferred to a suitable substrate (glass slide or aluminum foil) for further studies. An optical micrograph of the film (shown in Figure S13) demonstrates its transparent nature. Surprisingly, the FESEM micrograph (Figure 2b and S14) reveals an assembly of vertically aligned nanoplates with a thickness of 200 ± 100 nm and an edge length of 600 ± 200 nm. Atomic force microscopy (AFM) analysis of the assembly of vertically aligned nanoplates gave more insights into the morphology. The nanoplates were found to have a thickness of 200 ± 100 nm with a width of 450 ± 200 nm (Figure S15). An expanded view of the image suggests the vertical alignment of most of the platelets (Figure 2c). FESEM images collected from different cluster batches demonstrated the reproducibility of these nanostructures (Figure S16). We note that the oriented assembly of nanoclusters leading to specific morphology, such as nanosheets, fibers, *etc.*, was observed earlier.[37−40]

UV–vis absorption studies of the dissolved ESD film showed well-defined absorption features matching with the as-synthesized cluster (Figure S17a). ESI-MS of the ESD film showed a peak at m/z 3213.96 in the positive ion mode which matches well with the molecular composition of the Co_6 cluster (Figure S17b). Solid-state IR studies were carried out on both the drop-casted cluster and the ESD film, and both were in good agreement (Figure S18). These results concluded that the cluster remains intact upon ESD. To ensure the uniqueness of the ESD technique, we drop-casted the same cluster solution (in DCM) onto a water surface. FESEM images of the films formed reveal no specific morphology, inferring that nanoplates are specific to the deposition technique (Figure S19). The formation of nanoplates using ESD is also substrate specific, and we have confirmed it by taking different substrates such as conducting carbon cloth, glycerol, and ethylene glycol (Figures S20, S21, and S22). This signifies that the use of a liquid hydrophilic substrate is essential to create such nanostructures. This oriented microcrystalline assembly could be a result of specific intramolecular interactions. To further understand such interactions, we have carried out periodic DFT calculations.[41] We have considered a dimer constituted by two $[Co_6S_8(DPPE)_6Cl_6]$ units and analyzed the energetics of its formation from two monomer units for studying the role of intercluster interactions with and

https://doi.org/10.1021/acsmaterialslett.3c00085
ACS Materials Lett. 2023, 5, 893–899

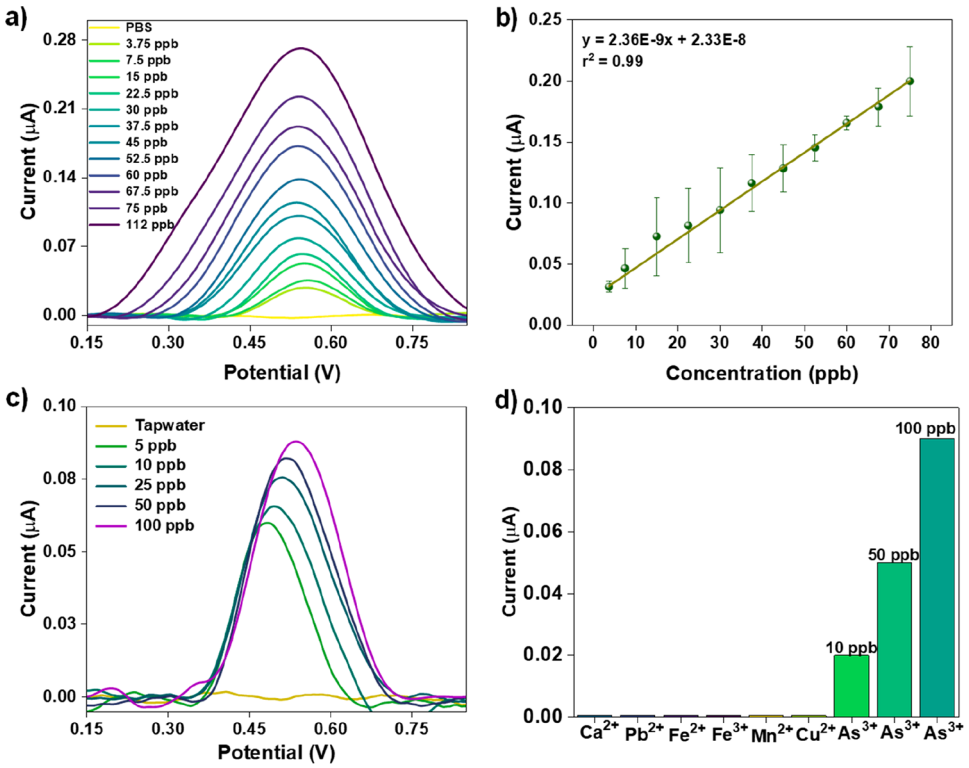

Figure 3. (a) Baseline corrected voltammetric profiles of the ESD-modified Co_6 GC electrode in response to various concentrations (3.75−112 ppb) of As^{3+} in a buffer solution. (b) Linearity analysis of voltammetric response for different concentrations of As^{3+}. Error bars represent interelectrode variability. (c) Baseline corrected voltammetric profiles for various concentrations (5−100 ppb) of As^{3+} in tap water. (d) Interfering ion studies with different metal ions (100 ppb each of Ca^{2+}, Pb^{2+}, Fe^{2+}, Fe^{3+}, Mn^{2+}, and Cu^{2+} added sequentially) and the response of arsenic in the presence of all of the metal ions.

without van der Waals (vdW) considerations.[42] The calculated dimer formation energy when vdW interactions are taken into account is found to be less than the non-vdW scenario by 2.03 eV (optimized structure is in Figure 2e). This indicates that the noncovalent interactions such as CH···Cl and CH···π mediated by the phenyl rings of ligands provide structural stability of the superstructure (Figure 2f,g).

These oriented nanoplates were cast on a glassy carbon (GC) electrode using 5 wt % nafion, and the deposited film contained intact nanoplates (Figure S23). Electrochemical arsenic (As^{3+}) sensing experiments were carried out using voltammetry. The experimental details are presented in the SI. Different concentrations of As^{3+} were prepared by dissolving $NaAsO_2$ in phosphate-buffered saline (PBS, pH ∼ 7). The electrode showed an excellent current response to As^{3+} in PBS as shown in Figure 3a, over a wide concentration window of 4 to 112 ppb. The electrode system is stable for multiple measurements, and all of the concentration-dependent measurements shown in Figures 3a and S24 were performed using a single electrode. The increase in current upon increasing the concentration is due to enhanced electrocatalytic oxidation of arsenite onto the exposed nanoplates. Control experiments were also performed for bare GC electrode and as-synthesized Co_6 cluster (Figures S25 and S26). No significant current response was observed for these experiments. Vertically aligned nanoplates with specific exposed planes and consequent cluster sites probably act as catalytically active surfaces for As^{3+} binding.

We have investigated the suitable binding of $As(OH)_3$ with the Co_6 cluster using DFT calculations, which reveals that $As(OH)_3$ exhibits a strong affinity to the cluster with a binding energy of −0.63 eV in correspondence with the experimental observation (Figure S27). It may be noted that arsenite exists as the neutral $As(OH)_3$ species at pH 7. This is further supported by the charge density difference (CDD) analysis of $As(OH)_3$ binding to the Co_6 cluster (Figure S28). Detailed structural analysis uncovers that the phosphine end of the ligand bonded with cobalt has a high affinity with As^{3+}. Although the free phosphine end interacts with As^{3+}, the cavity made by the flexible arms of DPPE interacts with the −OH of $As(OH)_3$ (shown in Figure S29a). Bader charge analysis of the $Co_6S_8P_6$ unit reveals that all P atoms bonded with the Co are negatively charged, which favors electrostatic interaction with the positively charged arsenic (Figure S29b).

The sensor behaves linearly in the concentration window relevant to drinking water. The sensitivity was calculated to be 3.496×10^{-9} μA/ppb/mm^2, and the estimated limit of detection (LOD) was 0.66 ppb, which is far below the guideline value of arsenic in drinking water (10 ppb), as recommended by the World Health Organization (WHO).[43,44] A theoretical LOD of 0.825 ppb using CoOx on a glassy carbon electrode in PBS at pH 7 was reported previously.[31] Similar experiments were conducted in tap water with the gradual addition of As^{3+} over a concentration window of 5−100 ppb (Figure 3c). As may be inferred from this data set, measurements below 10 ppb can be done easily in field conditions. Interference studies with different metal ions, commonly present in arsenic-contaminated water, were performed in tap water (Figure 3d) and PBS (Figure S30). The concentration of all of the metal ions (Ca^{2+} Mn^{2+}, Fe^{2+}, Fe^{3+}, Cu^{2+}, and Pb^{2+}) was maintained at 100 ppb each during the studies. Later, we analyzed three arsenic concentrations

https://doi.org/10.1021/acsmaterialslett.3c00085
ACS Materials Lett. 2023, 5, 893−899

(10, 50, and 100 ppb) which were added sequentially in the presence of these ions at 100 ppb each. The electrode responds specifically to As^{3+} both in tap water and in PBS. The recyclability of the working electrode for arsenic detection was verified by performing cyclic voltammetry (CV) in PBS for 40 cycles with a fixed arsenite concentration of 100 ppb (Figure S31). The composition of the nanoplates after electrochemical arsenic sensing experiments was verified by UV−vis measurement (Figure S32). The tests conducted individually and collectively show the specificity and practical utility of the sensor.

The analysis can be performed without the need for preconcentration, additional reagents, and sample processing, which enables rapid measurements. From a practical perspective, the amount of cobalt cluster in an electrode is approximately 0.5 ng. With the cost of the binder and other consumables, the materials cost per electrode is expected to be less than $0.5. As the electrode can be reused, costs can come down further. Therefore, each analysis can be done below a cost of $1.

In conclusion, we present a practical arsenic sensing method built using an atomically precise Co_6 cluster working down to 5 ppb in tap water. A new cobalt cluster, $[Co_6S_8DPPE_6Cl_6]$, was synthesized using ambient conditions and characterized using SCXRD and other spectroscopic studies. The sensing platform was prepared by ESD of the cluster on the water surface resulting in vertically aligned crystalline nanoplates. The interactions of charged microdroplets of cluster ions with the water surface resulted in the preferential organization of these nanoplates, enhancing the surface area and selectivity leading to an excellent response to As^{3+}. We obtained a LOD of 0.66 ppb, which is well below the guideline value of arsenic in drinking water (10 ppb) as recommended by WHO. Ease of availability, selectivity, sensitivity, and cost-effectiveness made it a good candidate for practical arsenic sensing. We note that affordable arsenic sensing below 10 ppb in water can have far reaching implications for global health.

■ ASSOCIATED CONTENT

Supporting Information

The Supporting Information is available free of charge at https://pubs.acs.org/doi/10.1021/acsmaterialslett.3c00085.

Experimental details, instrumentation, theoretical calculations, crystal data, characterization of the cluster by UV−vis, ESI-MS, SEM, XPS, PXRD, and TGA; characterization of ESD film by UV−vis, ESI-MS, AFM, SEM, and FTIR; CV of control experiments of arsenic sensing (PDF)

Crystallographic information (CIF)

■ AUTHOR INFORMATION

Corresponding Authors

Thalappil Pradeep − *Department of Chemistry, DST Unit of Nanoscience (DST UNS) and Thematic Unit of Excellence (TUE), Indian Institute of Technology Madras, Chennai 600036, India; International Centre for Clean Water, Chennai 600113, India;* orcid.org/0000-0003-3174-534X; Email: pradeep@iitm.ac.in

Biswarup Pathak − *Department of Chemistry, Indian Institute of Technology Indore (IIT Indore), Indore 453552, India;* orcid.org/0000-0002-9972-9947; Email: biswarup@iiti.ac.in

Authors

Anagha Jose − *Department of Chemistry, DST Unit of Nanoscience (DST UNS) and Thematic Unit of Excellence (TUE), Indian Institute of Technology Madras, Chennai 600036, India*

Arijit Jana − *Department of Chemistry, DST Unit of Nanoscience (DST UNS) and Thematic Unit of Excellence (TUE), Indian Institute of Technology Madras, Chennai 600036, India*

Tanvi Gupte − *Department of Chemistry, DST Unit of Nanoscience (DST UNS) and Thematic Unit of Excellence (TUE), Indian Institute of Technology Madras, Chennai 600036, India;* orcid.org/0000-0002-0518-8482

Akhil S. Nair − *Department of Chemistry, Indian Institute of Technology Indore (IIT Indore), Indore 453552, India;* orcid.org/0000-0001-5723-3970

Keerthana Unni − *Department of Chemistry, DST Unit of Nanoscience (DST UNS) and Thematic Unit of Excellence (TUE), Indian Institute of Technology Madras, Chennai 600036, India*

Ankit Nagar − *Department of Chemistry, DST Unit of Nanoscience (DST UNS) and Thematic Unit of Excellence (TUE), Indian Institute of Technology Madras, Chennai 600036, India*

Amoghavarsha R. Kini − *Department of Chemistry, DST Unit of Nanoscience (DST UNS) and Thematic Unit of Excellence (TUE), Indian Institute of Technology Madras, Chennai 600036, India*

B. K. Spoorthi − *Department of Chemistry, DST Unit of Nanoscience (DST UNS) and Thematic Unit of Excellence (TUE), Indian Institute of Technology Madras, Chennai 600036, India*

Sourav Kanti Jana − *Department of Chemistry, DST Unit of Nanoscience (DST UNS) and Thematic Unit of Excellence (TUE), Indian Institute of Technology Madras, Chennai 600036, India;* orcid.org/0000-0001-5772-7022

Complete contact information is available at: https://pubs.acs.org/10.1021/acsmaterialslett.3c00085

Author Contributions

A. Jose performed synthesis, crystallization, and other experimental studies. A. Jana, K.U., and B.K.S. performed electrospray deposition studies. T.G., A. Jose, and A. Jana performed electrochemical sensing studies. A.S.N. performed theoretical calculations under the guidance of B.P. A.N. performed FESEM studies. A.R.K. performed crystallization and X-ray photoelectron spectroscopic studies. S.K.J. was involved in the discussion of experimental data A. Jose wrote the first draft of the manuscript with inputs from T.P. and A. Jana, and all coauthors contributed to finalizing it. T.P. conceptualized the work and finalized the manuscript. CRediT: **Anagha Jose** conceptualization, investigation, writing-original draft; **Keerthana Unni** investigation.

Notes

The authors declare no competing financial interest.

■ ACKNOWLEDGMENTS

We thank the Sophisticated Analytical Instruments Facility, IIT Madras, and Sudhadevi Antharjanam for the SC-XRD measurements. A.J. thanks MHRD for the PMRF research grant. T.P. acknowledges funding from the Centre of Excellence on Molecular Materials and Functions under the

Institution of Eminence scheme of IIT Madras. We thank the Department of Science and Technology, Government of India, for continuous support of our research program.

REFERENCES

(1) Chakraborty, I.; Pradeep, T. Atomically Precise Clusters of Noble Metals: Emerging Link between Atoms and Nanoparticles. *Chem. Rev.* **2017**, *117*, 8208−8271.
(2) Kang, X.; Li, Y.; Zhu, M.; Jin, R. Atomically Precise Alloy Nanoclusters: Syntheses, Structures, and Properties. *Chem. Soc. Rev.* **2020**, *49*, 6443−6514.
(3) Murray, R. W. Nanoelectrochemistry: Metal Nanoparticles, Nanoelectrodes, and Nanopores. *Chem. Rev.* **2008**, *108*, 2688−2720.
(4) Zhu, Y.; Lin, Q.; Zhong, Y.; Tahini, H. A.; Shao, Z.; Wang, H. Metal Oxide-Based Materials as an Emerging Family of Hydrogen Evolution Electrocatalysts. *Energy Environ. Sci.* **2020**, *13*, 3361−3392.
(5) Chen, X.; Mao, S. S. Titanium Dioxide Nanomaterials: Synthesis, Properties, Modifications and Applications. *Chem. Rev.* **2007**, *107*, 2891−2959.
(6) Roy, X.; Lee, C. H.; Crowther, A. C.; Schenck, C. L.; Besara, T.; Lalancette, R. A.; Siegrist, T.; Stephens, P. W.; Brus, L. E.; Kim, P.; Steigerwald, M. L.; Nuckolls, C. Nanoscale Atoms in Solid-State Chemistry. *Science.* **2013**, *341*, 157−160.
(7) Gadjieva, N. A.; Champsaur, A. M.; Steigerwald, M. L.; Roy, X.; Nuckolls, C. Dimensional Control of Assembling Metal Chalcogenide Clusters. *Eur. J. Inorg. Chem.* **2020**, *2020*, 1245−1254.
(8) Gholipour-Ranjbar, H.; Fang, H.; Guan, J.; Peters, D.; Seifert, A.; Jena, P.; Laskin, J. Designing New Metal Chalcogenide Nanoclusters through Atom-by-Atom Substitution. *Small* **2021**, *17*, 2002927.
(9) Jin, R. Atomically Precise Metal Nanoclusters: Stable Sizes and Optical Properties. *Nanoscale* **2015**, *7*, 1549−1565.
(10) Hulkko, E.; Lopez-Acevedo, O.; Koivisto, J.; Levi-Kalisman, Y.; Kornberg, R. D.; Pettersson, M.; Häkkinen, H. Electronic and Vibrational Signatures of the Au102(p -MBA) 44 Cluster. *J. Am. Chem. Soc.* **2011**, *133*, 3752−3755.
(11) Du, X.; Jin, R. Atomically Precise Metal Nanoclusters for Catalysis. *ACS Nano* **2019**, *13*, 7383−7387.
(12) Jain, P. K.; Huang, X.; El-Sayed, I. H.; El-Sayed, M. A. Noble Metals on the Nanoscale: Optical and Photothermal Properties and Some Applications in Imaging, Sensing, Biology, and Medicine. *Acc. Chem. Res.* **2008**, *41*, 1578−1586.
(13) Ye, R.; Hurlburt, T. J.; Sabyrov, K.; Alayoglu, S.; Somorjai, G. A. Molecular Catalysis Science: Perspective on Unifying the Fields of Catalysis. *Proc. Natl. Acad. Sci. U. S. A.* **2016**, *113*, 5159−5166.
(14) Zhu, M.; Aikens, C. M.; Hendrich, M. P.; Gupta, R.; Qian, H.; Schatz, G. C.; Jin, R. Reversible Switching of Magnetism in Thiolate-Protected Au 25 Superatoms. *J. Am. Chem. Soc.* **2009**, *131*, 2490−2492.
(15) Kang, X.; Zhu, M. Tailoring the Photoluminescence of Atomically Precise Nanoclusters. *Chem. Soc. Rev.* **2019**, *48*, 2422−2457.
(16) Wang, X.; Zhao, L.; Li, X.; Liu, Y.; Wang, Y.; Yao, Q.; Xie, J.; Xue, Q.; Yan, Z.; Yuan, X.; Xing, W. Atomic-Precision Pt6 Nanoclusters for Enhanced Hydrogen Electro-Oxidation. *Nat. Commun.* **2022**, *13*, 1−10.
(17) Du, Y.; Sheng, H.; Astruc, D.; Zhu, M. Atomically Precise Noble Metal Nanoclusters as Efficient Catalysts: A Bridge between Structure and Properties. *Chem. Rev.* **2020**, *120*, 526−622.
(18) Chen, X.; Zhou, Y.; Peng, X.; Yoon, J. Fluorescent and Colorimetric Probes for Detection of Thiols. *Chem. Soc. Rev.* **2010**, *39*, 2120−2135.
(19) Guan, G.; Zhang, S. Y.; Cai, Y.; Liu, S.; Bharathi, M. S.; Low, M.; Yu, Y.; Xie, J.; Zheng, Y.; Zhang, Y. W.; Han, M. Y. Convenient Purification of Gold Clusters by Co-Precipitation for Improved Sensing of Hydrogen Peroxide, Mercury Ions and Pesticides. *Chem. Commun.* **2014**, *50*, 5703−5705.
(20) March, G.; Nguyen, T. D.; Piro, B. Modified Electrodes Used for Electrochemical Detection of Metal Ions in Environmental Analysis. *Biosensors* **2015**, *5*, 241−275.
(21) Mathew, A.; Pradeep, T. Noble Metal Clusters: Applications in Energy, Environment, and Biology. *Part. Part. Syst. Charact.* **2014**, *31*, 1017−1053.
(22) Yorov, K. E.; Mir, W. J.; Song, X.; Gutiérrez-Arzaluz, L.; Naphade, R.; Nematulloev, S.; Chen, C.; Huang, R.-W.; Shao, B.; Hasanov, B. E.; Han, Y.; Mohammed, O. F.; Bakr, O. M. Mn^{4+}-Doped Fluoride Nanocrystals Enable High-Resolution Red-Emitting X-Ray Imaging Screens. *ACS Materials Lett.* **2022**, *4*, 2273−2281.
(23) Male, K. B.; Hrapovic, S.; Santini, J. M.; Luong, J. H. T. Biosensor for Arsenite Using Arsenite Oxidase and Multiwalled Carbon Nanotube Modified Electrodes. *Anal. Chem.* **2007**, *79*, 7831−7837.
(24) Ravenscroft, P. *Predicting the Global Extent of Arsenic Pollution of Groundwater and Its Potential Impact on Human Health*; UNICEF: New York, 2007.
(25) Podgorski, J.; Berg, M. Global Threat of Arsenic in Groundwater. *Science.* **2020**, *368*, 845−850.
(26) Yang, M.; Chen, X.; Jiang, T. J.; Guo, Z.; Liu, J. H.; Huang, X. J. Electrochemical Detection of Trace Arsenic(III) by Nanocomposite of Nanorod-Like α-MnO2 Decorated with ∼ 5 nm Au Nanoparticles: Considering the Change of Arsenic Speciation. *Anal. Chem.* **2016**, *88*, 9720−9728.
(27) Jana, S. K.; Chaudhari, K.; Islam, M. R.; Natarajan, G.; Ahuja, T.; Som, A.; Paramasivam, G.; Raghavendra, A.; Sudhakar, C.; Pradeep, T. Selective and Practical Graphene-Based Arsenite Sensor at 10 ppb. *ACS Appl. Nano Mater.* **2022**, *5*, 11876−11888.
(28) Gupte, T.; Jana, S. K.; Mohanty, J. S.; Srikrishnarka, P.; Mukherjee, S.; Ahuja, T.; Sudhakar, C.; Thomas, T.; Pradeep, T. Highly Sensitive As3+ Detection Using Electrodeposited Nanostructured MnOx and Phase Evolution of the Active Material during Sensing. *ACS Appl. Mater. Interfaces* **2019**, *11*, 28154−28163.
(29) Jiang, T. J.; Guo, Z.; Liu, J. H.; Huang, X. J. Gold Electrode Modified with Ultrathin SnO2 Nanosheets with High Reactive Exposed Surface for Electrochemical Sensing of As(III). *Electrochim. Acta* **2016**, *191*, 142−148.
(30) Kwak, K.; Lee, D. Electrochemistry of Atomically Precise Metal Nanoclusters. *Acc. Chem. Res.* **2019**, *52*, 12−22.
(31) Salimi, A.; Mamkhezri, H.; Hallaj, R.; Soltanian, S. Electrochemical Detection of Trace Amount of Arsenic(III) at Glassy Carbon Electrode Modified with Cobalt Oxide Nanoparticles. *Sensors Actuators, B Chem.* **2008**, *129*, 246−254.
(32) Sarkar, D.; Mahapatra, A.; Som, A.; Kumar, R.; Nagar, A.; Baidya, A.; Pradeep, T. Patterned Nanobrush Nature Mimics with Unprecedented Water-Harvesting Efficiency. *Adv. Mater. Interfaces* **2018**, *5*, 1800667.
(33) Jana, A.; Jana, S. K.; Sarkar, D.; Ahuja, T.; Basuri, P.; Mondal, B.; Bose, S.; Ghosh, J.; Pradeep, T. Electrospray Deposition-Induced Ambient Phase Transition in Copper Sulphide Nanostructures. *J. Mater. Chem. A* **2019**, *7*, 6387−6394.
(34) Ray Chowdhuri, A.; Spoorthi, B. K.; Mondal, B.; Bose, P.; Bose, S.; Pradeep, T. Ambient Microdroplet Annealing of Nanoparticles. *Chem. Sci.* **2021**, *12*, 6370−6377.
(35) Stuczynski, S. M.; Kwon, Y. U.; Steigerwald, M. L. The Use of Phosphine Chalcogenides in the Preparation of Cobalt Chalcogenides. *J. Organomet. Chem.* **1993**, *449*, 167−172.
(36) Frisch, M. J.; Trucks, G. W.; Schlegel, H. B.; Scuseria, G. E.; Robb, M. A.; Cheeseman, J. R.; Scalmani, G.; Barone, V.; Mennucci, B.; Petersson, G. A.; Nakatsuji, H.; et al.. *Gaussian 09*, Revision D.01; Gaussian, Inc.: Wallingford, CT, 2009.
(37) Som, A.; Griffo, A.; Chakraborty, I.; Hähl, H.; Mondal, B.; Chakraborty, A.; Jacobs, K.; Laaksonen, P.; Ikkala, O.; Pradeep, T.; Nonappa. Strong and Elastic Membranes via Hydrogen Bonding Directed Self-Assembly of Atomically Precise Nanoclusters. *Small* **2022**, *18*, 2201707.
(38) Xie, Z.; Sun, P.; Wang, Z.; Li, H.; Yu, L.; Sun, D.; Chen, M.; Bi, Y.; Xin, X.; Hao, J. Metal−Organic Gels from Silver Nanoclusters with

Aggregation-Induced Emission and Fluorescence-to-Phosphorescence Switching. *Angew. Chemie - Int. Ed.* **2020**, *59*, 9922−9927.
(39) Wu, Z.; Dong, C.; Li, Y.; Hao, H.; Zhang, H.; Lu, Z.; Yang, B. Self-Assembly of Au15 into Single-Cluster-Thick Sheets at the Interface of Two Miscible High-Boiling Solvents. *Angew. Chemie - Int. Ed.* **2013**, *52*, 9952−9955.
(40) Wu, Z.; Liu, J.; Li, Y.; Cheng, Z.; Li, T.; Zhang, H.; Lu, Z.; Yang, B. Self-Assembly of Nanoclusters into Mono-, Few-, and Multilayered Sheets via Dipole-Induced Asymmetric van Der Waals Attraction. *ACS Nano* **2015**, *9*, 6315−6323.
(41) Kresse, G.; Hafner, J. Ab Initio Molecular-Dynamics Simulation of the Liquid-Metal−Amorphous-Semiconductor Transition in Germanium. *Phys. Rev. B: Condens. Matter Mater. Phys.* **1994**, *49*, 14251.
(42) Grimme, S. *J. Comput. Chem.* **2006**, *27*, 1787−1799.
(43) WHO. *Guidelines for Drinking-Water Quality*; WHO, 2011; pp 315−318.
(44) U.S. EPA. Technical Factsheet: Final Rule for Arsenic in Drinking Water; U.S. EPA, 2001; pp 1−6.

https://doi.org/10.1021/acsmaterialslett.3c00085
ACS Materials Lett. 2023, 5, 893−899